



Development of new $Zr_xTi_{1-x}P_2O_7$ materials as model compounds for the recycling of metallic waste from phosphate chemistry

I. Maârouf^{1*}, A. Oulmekki¹, J. Toyir², M. Nawdali², I. Zarguili², H. El Ghadraoui¹

¹Laboratoire de Chimie de la matière condensée, Faculté des Sciences et Techniques Fès, Université Sidi Mohammed Ben Abdellah, B.P. 2202 Maroc

²Equipe de recherche en procédés pour l'énergie et l'environnement, Laboratoire de Chimie de la matière condensée, Faculté Polydisciplinaire Taza, Université Sidi Mohammed Ben Abdellah, B.P. 1223 Taza Maroc

Received 8 Jan 2017
Revised 16 Apr 2017
Accepted 18 Apr 2017

Keywords

- ✓ Pyrophosphate,
- ✓ Zirconium,
- ✓ Titanium,
- ✓ M-P-O,
- ✓ Metal trace element,

[*maaroufismail@gmail.com](mailto:maaroufismail@gmail.com)

Phone: +212 6 74 78 71 91

Abstract

In this work, new protocols for the synthesis of M-P-O materials were developed for the recycling of phosphates as well as to trap metal trace elements, hazardous pollutants resulting from the phosphate industry. For this purpose, we have developed a simple and efficient process to synthesize new series of compounds $Zr_xTi_{1-x}P_2O_7$ ($0 < x < 1$). These pyrophosphates were prepared by solid-state synthesis and treated at different temperatures up to 900°C. The obtained materials were characterized by X-ray diffraction (XRD), scanning electron microscopy (SEM) and Infrared Spectroscopy (IR).

1. Introduction

The processes currently used in phosphate based industry generate substantial solid waste quantities containing dangerous substances such as Metallic Trace Elements (MTEs), which, beyond the permitted concentrations, are known to be very harmful to the environment and health [1,2]. The MTEs (eg Cd, Cr, Zn, Pb, Cu) extraction may result from dust emitted during the drying or calcination operation units and may also originate from the mineral sludge generated after the washing step [3]. Accordingly, the present investigation is associated to the strategic national plan of phosphate valorization through chemical recycling using phosphate based matrix as useful carriers for metallic trace elements [4]. The recycling processes have to be more efficient without negative impact on the environment. The MTEs harmful species captured under strict control can be combined with inorganic phosphates to produce useful advanced multifunctional materials for green chemistry applications and particularly for selective heterogeneous catalysis [5-7]. This chemistry route is favored by the capacity of the tetrahedral group PO_4^{3-} to bind with other structural units particularly those including metallic ions such as Fe^{2+} , Pb^{2+} [7,8] and Co^{2+} [9], previously studied in our laboratory. These studies have shown that PO_4^{3-} and MO_6 sequences ensure an appropriate space where the metal cations can fit properly. In addition, the exposed [100] planes associated with host cavities facilitate the insertion of metal counter anions. This study describes the different steps for developing an easy and efficient processes to synthesize new M-P-O compounds based on Fe, Pb, Cu, Ba, Zr, and Ti, in particular the series of compounds $Zr_xTi_{1-x}P_2O_7$ ($0 < x < 1$) prepared using free-solvent solid state route. Structural and physico-chemical properties of $Zr_xTi_{1-x}P_2O_7$ materials are determined using X-ray diffraction (XRD), scanning electron microscopy (SEM) and Infrared Spectroscopy (IR).

2. Experimental

2.1. Synthesis of $Zr_xTi_{1-x}P_2O_7$ materials

ZrP_2O_7 and TiP_2O_7 were prepared through solid-state method so-called “dry route” (absence of solvent) from a stoichiometric mixture (1/2) of $ZrO_2/(NH_4)_2HPO_4$ and $TiO_2/(NH_4)_2HPO_4$, respectively [10]. The reagents provided by Sigma-Aldrich are of analytical grade (99% purity). First, the appropriate amounts of starting products were mixed mechanically until a fine and homogeneous powder was obtained. Thermal pretreatment of powder was then operated as follows: isothermal heating at 200°C during 3 hours followed by a grinding step prior to increase temperature to 300°C and operating a second isothermal heating at this temperature for 4 hours. Subsequently, calcination of pretreated powder consisting of intermediate hydroxyphosphate compounds was carried by increasing the temperature from 300°C to 700°C (5°/min) and then 900°C following isothermal treatments for each temperature for 6 hours.

$Zr_xTi_{1-x}P_2O_7$ materials ($0 < x < 1$) synthesis was conducted according to the same procedure using a predefined $ZrO_2/TiO_2/(NH_4)_2HPO_4$ /mixtures corresponding to the stoichiometry of each compound in the $Zr_xTi_{1-x}P_2O_7$ series.

2.2. Characterization of $Zr_xTi_{1-x}P_2O_7$ materials

X-ray powder diffraction (XRD) analysis was carried out using an X'Pert High Score PAN analytical diffractometer equipped with a Cu $K\alpha_1$ radiation source ($\lambda = 1.5406 \text{ \AA}$). The XRD patterns were collected between $2\theta = 10^\circ$ and $2\theta = 80^\circ$, with a step width of 0.067° and counting 50s at each step. The scanning electron microscopy (SEM) images were collected on a FEI-quanta 200 instrument with an acceleration voltage of 20 kV. The preparation of the samples goes through a dehydration step and then a heat treatment. Afterwards, the samples were pressed into pellets with a diameter of 13 mm and a thickness of 1 mm before analysis. Infrared spectroscopy (IR) spectra were recorded on a JASCO-4100FT-IR spectrometer equipped with a standard laser source and a TGS detector. The spectrum was recorded in transmission mode from 4000 to 400 cm^{-1} at a resolution of 2 cm^{-1} and a scanning speed of 2 mm/sec. The sample pellet (13 mm in diameter and 1 mm in thickness) was prepared by pressing a mixture of sample (10 wt%) and KBr (90 wt%).

3. Results and discussion

3.1. XRD analysis

In a first step, ZrP_2O_7 and TiP_2O_7 were characterized by X-ray diffraction to confirm their crystalline phases serving as references for XRD patterns of each compound in the $Zr_xTi_{1-x}P_2O_7$ series. Figure 1 shows X-ray diffraction profiles for ZrP_2O_7 and TiP_2O_7 . The most intense characteristic diffraction lines appear for ZrP_2O_7 at diffraction angles $2\theta = 18.67, 21.61, 24.15, 26.56, 30.70, 36.18^\circ$ indexed to diffraction planes hkl (111) (200) (210) (211) (311) respectively [11]. Concerning TiP_2O_7 , the profile is different with diffraction angles for the most intense lines of respective values $2\theta = 19.54, 22.61, 25.35, 27.83, 32.17, 37.92^\circ$ corresponding to the diffraction planes hkl (511) (600) (630) (721) (660) (933) respectively [12].

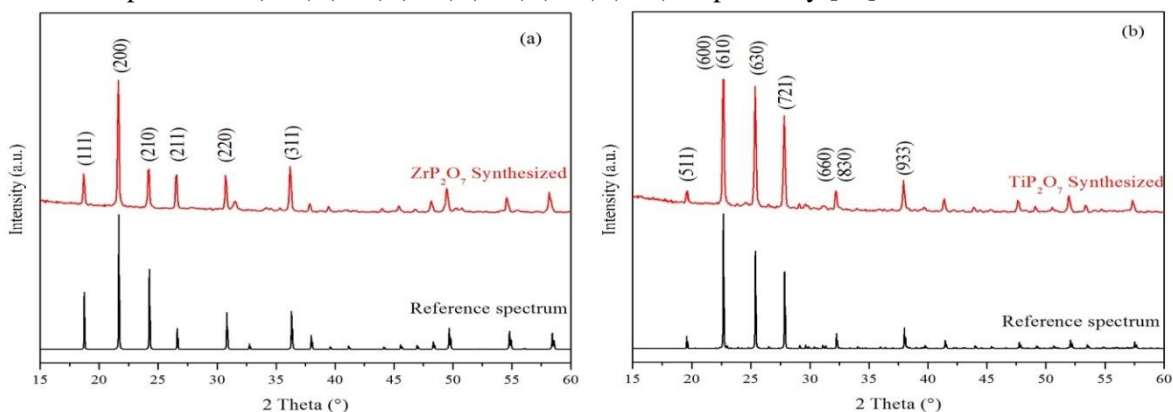


Figure 1: X-ray diffractograms of (a) ZrP_2O_7 and (b) TiP_2O_7

In comparison with the literature data, the preliminary X-ray diffraction results on the prepared ZrP_2O_7 and TiP_2O_7 samples show identical structures as previously published [13,14]. It was confirmed that these compounds crystallize in a cubic space group system Pa3 with $a = 8.22 \text{ \AA}$ for ZrP_2O_7 and $a = 23.56 \text{ \AA}$ for TiP_2O_7 . The parameters of the synthesized samples are presented in Table 1.

Table 1: Comparison of ZrP_2O_7 and TiP_2O_7 unit cells

	Crystal structure	Space group	Parameter $a^{(1)}$	Parameter $a^{(2)}$
ZrP_2O_7	Cubic	Pa3	$a = 8.223 (6) \text{ \AA}$	$a = 8.200 \text{ \AA}$
TiP_2O_7	Cubic	Pa3	$a = 23.560 (2) \text{ \AA}$	$a = 23.534 \text{ \AA}$

(1) Values derived from this work

(2) Reported values ref. [13,14]

XRD results confirm the control of the experimental protocol (dry route) for the preparation of two well-defined reference materials. Based on these results, we proceeded with an experimental approach of progressive substitution of Zr by Ti and vice versa, to obtain $\text{Zr}_x\text{Ti}_{1-x}\text{P}_2\text{O}_7$ ($0 < x < 1$) compounds.

Diffraction patterns obtained from XRD analysis of $\text{Zr}_x\text{Ti}_{1-x}\text{P}_2\text{O}_7$ ($0 < x < 0.4$) series clearly indicate that all the compounds obtained crystallize in the same system as for TiP_2O_7 basic phosphate. So the conservation of the structure is ensured for this substitution range. The insertion of Zr into the TiP_2O_7 structure is optimal for a percentage of 20% Zr. Beyond this ratio, the phase is saturated and it is no longer possible to make additional Zr insertion. This is demonstrated by the XRD results showing the progressive formation of ZrO_2 beyond the indicated maximum insertion rate.

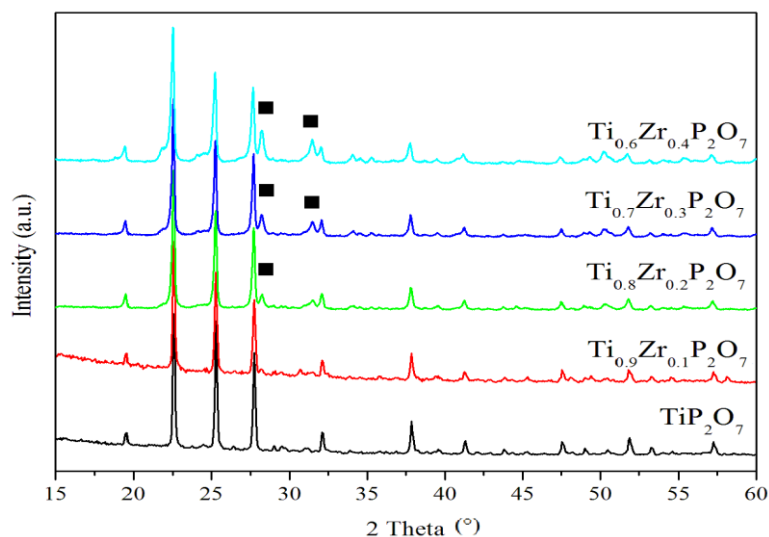


Figure 2: XRD patterns of $\text{Zr}_x\text{Ti}_{1-x}\text{P}_2\text{O}_7$ ($0 < x < 0.4$)
 ■ The characteristic peaks of ZrO_2

Figure 3 displays XRD patterns for the $\text{Zr}_x\text{Ti}_{1-x}\text{P}_2\text{O}_7$ series ($0.6 < x < 1$). In this case, solid-state synthesis effectively works for a substitution rate of Zr by Ti up to 20%. Above this percentage, an overlap of two peaks that shows a shoulder appears at about $2\theta = 30.7^\circ$ so that the initial phase of ZrP_2O_7 disappears due to its interaction with Ti. It is not worthy the appearance of TiP_2O_7 characteristic diffraction lines in XRD profile of $\text{Zr}_{0.6}\text{Ti}_{0.4}\text{P}_2\text{O}_7$, indicating only a partial insertion of engaged Ti into ZrP_2O_7 leading to $\text{Zr}_x\text{Ti}_{1-x}\text{P}_2\text{O}_7$ and TiP_2O_7 separate phases.

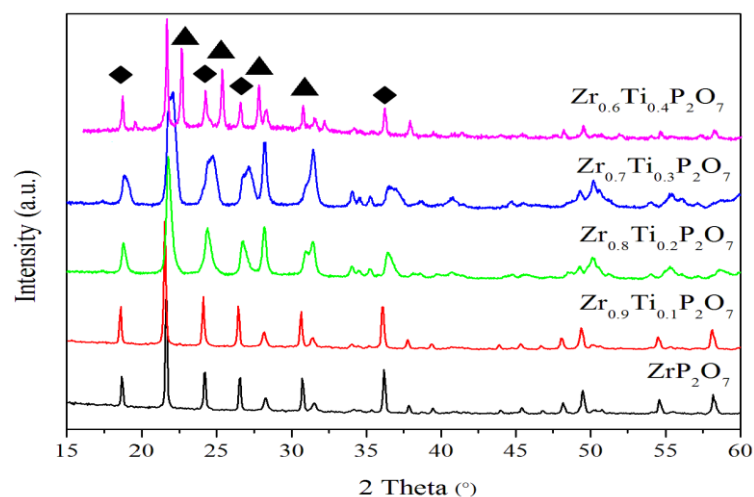


Figure 3: XRD pattern of $Zr_xTi_{1-x}P_2O_7$ ($0.6 < x < 1$)
 ▲ The characteristic peaks of TiP_2O_7
 ◆ The characteristic peaks of ZrP_2O_7

In order to deeply understand the structural impact of Ti (or Zr) insertion inside ZrP_2O_7 (or TiP_2O_7) matrix we followed the unit cell evolution. Table 2 summarizes the evolution of the cell parameter (a) for each compound. For $Zr_xTi_{1-x}P_2O_7$ ($0 < x < 0.2$), Zr insertion leads to an increase in parameter (a) from 23.56 to 23.59 Å, therefore a proportional increase in the volume is observed. In the case of the $Zr_xTi_{1-x}P_2O_7$ ($0.8 < x < 1$) series, the value of the parameter (a) decreased from 8.22 to 8.20 Å. The observed variations are consistent with the difference between the ionic radius of the two inserted elements which are 72pm for Zr and 61pm for Ti.

Tableau 2: Evolution of the unit cell parameter a as a function of the insertion rate

x	Compounds	Parameter a (Å) ± 0.001
0	TiP_2O_7	23,56
0.05	$Zr_{0.05}Ti_{0.95}P_2O_7$	23,58
0.1	$Zr_{0.1}Ti_{0.9}P_2O_7$	23,59
0.15	$Zr_{0.15}Ti_{0.85}P_2O_7$	23,59
0.2	$Zr_{0.2}Ti_{0.8}P_2O_7$	23,59
0.3 ^a	-	-
0.4 ^a	-	-
0.6 ^a	-	-
0.7 ^a	-	-
0.8	$Zr_{0.8}Ti_{0.2}P_2O_7$	8,20
0.85	$Zr_{0.85}Ti_{0.15}P_2O_7$	8,20
0.9	$Zr_{0.9}Ti_{0.1}P_2O_7$	8,21
0.95	$Zr_{0.95}Ti_{0.05}P_2O_7$	8,22
1	ZrP_2O_7	8,22

^a Compounds for which the substitution of Zr by Ti was not effective

3.2. SEM analysis

Scanning electron microscopy (SEM) was applied to various samples of the $Zr_xTi_{1-x}P_2O_7$ ($0 < x < 1$) series. SEM image of $Zr_{0.4}Ti_{0.6}P_2O_7$ (figure 4) displays globular aggregates with uniform particle size distribution. $Zr_{0.4}Ti_{0.6}P_2O_7$ mainly consists of crystals with sizes ranging from 1.228 and 5.419 μm whereas some particles of undefined forms can be observed. This finding indicates the complexity of Zr accommodating process by the host compound TiP_2O_7 . Furthermore, a clear contrast appearing in the SEM image of this compound is may be attributed to the presence of ZrO_2 in accordance with XRD results (figure 2), which could not interact during the solid-state synthesis [15].

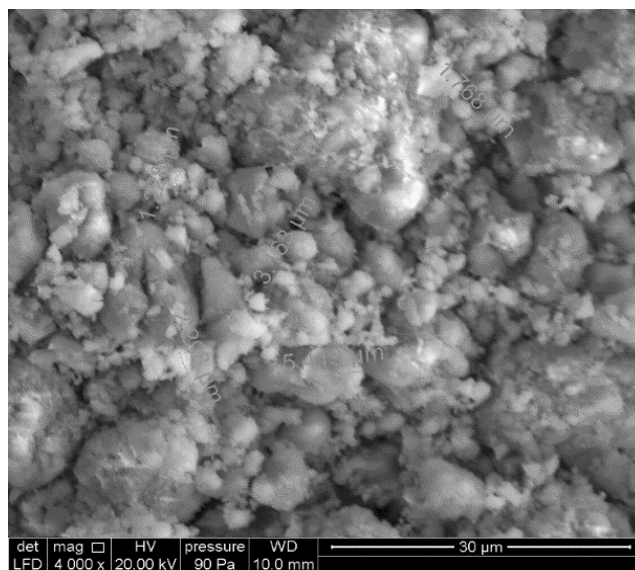


Figure 4: SEM image of $Zr_{0.4}Ti_{0.6}P_2O_7$

Figure 5 shows a compilation of representative SEM micrographs of TiP_2O_7 , $Zr_{0.1}Ti_{0.9}P_2O_7$ and $Zr_{0.8}Ti_{0.2}P_2O_7$. These compounds are composed of micrometric spherical particles with sizes ranging from 0.87 to 3.27 μm . Besides, few particles agglomerate together [16]. For the compounds showing substitution of Zr by Ti and vice versa ($Zr_xTi_{1-x}P_2O_7$ ($0 < x < 0.2$ or $0.8 < x < 1$)), the particle size is smaller and the contrast is less pronounced in comparison with the $Zr_xTi_{1-x}P_2O_7$ ($0.2 < x < 0.8$) compounds for which the insertion mechanism was not effective.

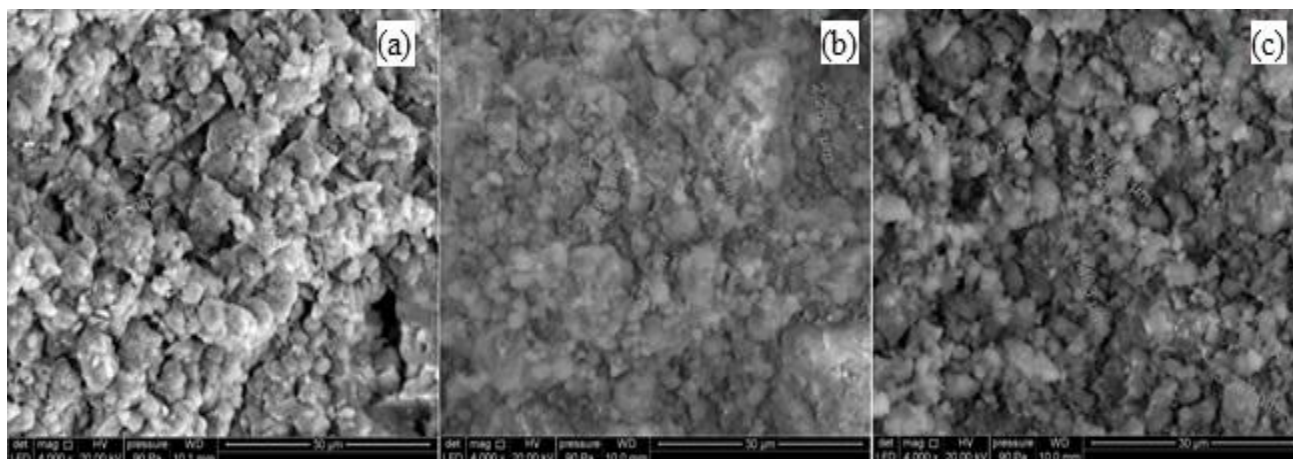


Figure 5: Representative SEM images of (a) TiP_2O_7 , (b) $Zr_{0.1}Ti_{0.9}P_2O_7$ and (c) $Zr_{0.8}Ti_{0.2}P_2O_7$.

3.3. IR spectroscopy

IR experiments were performed on samples of $Zr_xTi_{1-x}P_2O_7$ ($0 < x < 1$) series in order to demonstrate the presence of the (P_2O_7) groups in these compounds. Figure 6 represents the recorded FT-IR spectra for compounds showing the best substitution performance. It shows the presence of the characteristic bands associated with three vibrational domains $1400-1000\text{ cm}^{-1}$, $1000-700\text{ cm}^{-1}$ and $700-400\text{ cm}^{-1}$. No absorption bands assigned to H_2O are observed in FT-IR spectra indicating that our samples are anhydrous.

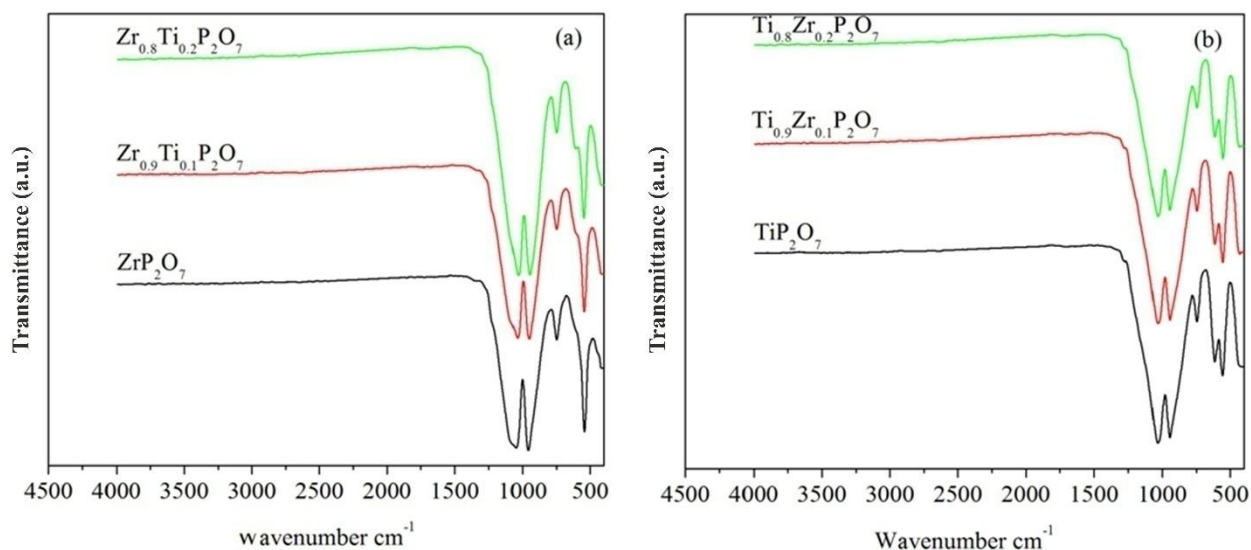


Figure 6: FT-IR spectra of (a) $Zr_xTi_{1-x}P_2O_7$ ($0.8 < x < 1$) and (b) $Zr_xTi_{1-x}P_2O_7$ ($0 < x < 0.2$)

FT-IR spectroscopy of the series $Zr_xTi_{1-x}P_2O_7$ ($0.8 < x < 1$)

In the $1400-1000\text{ cm}^{-1}$ et $700-400\text{ cm}^{-1}$ regions, figure 7 shows stretching vibrations (ν_s) at 1271 cm^{-1} and 1217 cm^{-1} and (ν_{as}) at 1088 cm^{-1} and 1047 cm^{-1} associated to the (PO_3) group [9,17,18]. The corresponding deformation modes are also visible at $576, 541, 450$ and 426 cm^{-1} [9,17].

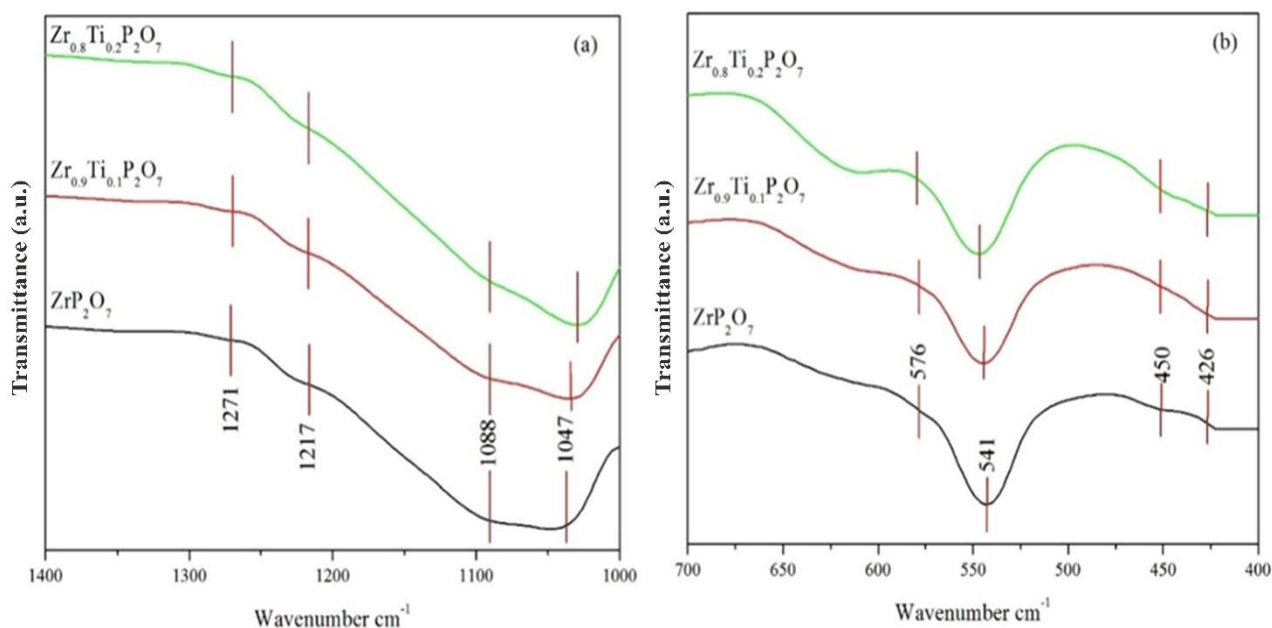


Figure 7: FT-IR spectra of ZrP_2O_7 , $Zr_{0.9}Ti_{0.1}P_2O_7$ and $Zr_{0.8}Ti_{0.2}P_2O_7$ (a) ($1400-1000\text{ cm}^{-1}$) and (b) ($700-400\text{ cm}^{-1}$)

Bands, appearing in the interval $1000-700\text{ cm}^{-1}$ (figure 8), correspond to the stretching vibrations of the (P_2O_7) groups displaying a bent POP bridge configuration [9]. In particular, the spectrum obtained on the ZrP_2O_7 -diphosphate reveals the presence of a band at 960 cm^{-1} attributed to antisymmetric stretching vibration ν_{as} (POP) and related band at 748 cm^{-1} due to the symmetric stretching vibration ν_s (POP) [18].

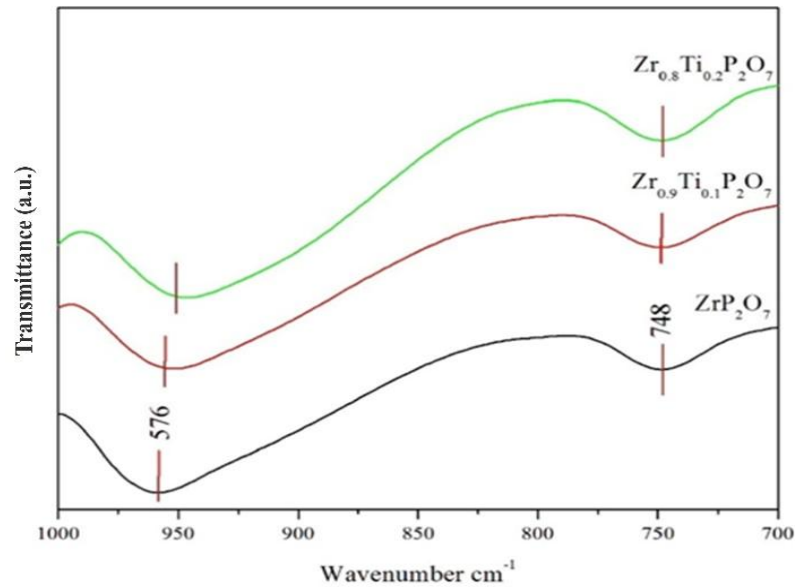


Figure 8: FT-IR spectra of ZrP_2O_7 ($1000-700cm^{-1}$)

FT-IR spectroscopy of the series $Zr_xTi_{1-x}P_2O_7$ ($0 < x < 0.2$)

For the $1400-1000\text{ cm}^{-1}$ and $700-400\text{ cm}^{-1}$ intervals, figure 9 shows the presence of stretching vibrations (ν_s) at 1276 cm^{-1} and stretching vibrations (ν_{as}) at 1029 cm^{-1} of the (PO_3) group [19]. Figure 9 also shows some of deformation modes of the (PO_3) group at 615 , 557 and 437 cm^{-1} [9,19].

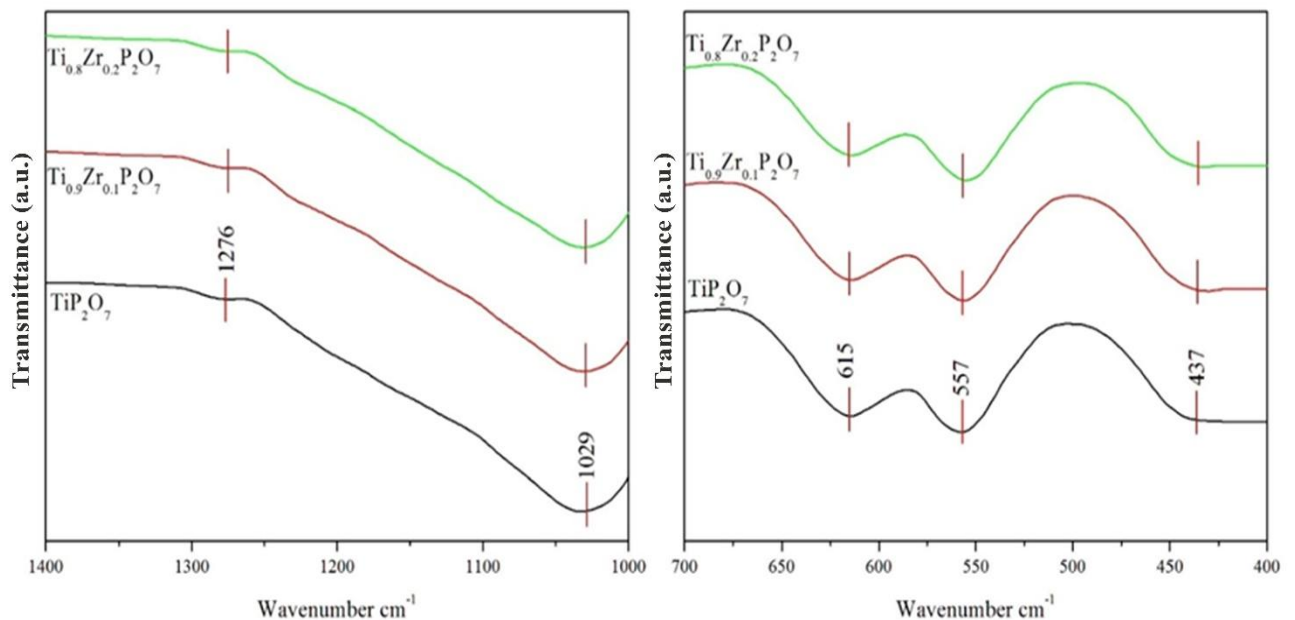


Figure 9: FT-IR spectra of TiP_2O_7 , $Ti_{0.9}Zr_{0.1}P_2O_7$ and $Ti_{0.8}Zr_{0.2}P_2O_7$
(a) ($1400-1000cm^{-1}$) and (b) ($700-400\text{ cm}^{-1}$)

Finally, in $1000-700\text{ cm}^{-1}$ region, figure 10 exhibits characteristic bands of stretching vibration modes $\nu_{as}(POP)$ and $\nu_s(POP)$ located at 945 cm^{-1} and 746 cm^{-1} [19].

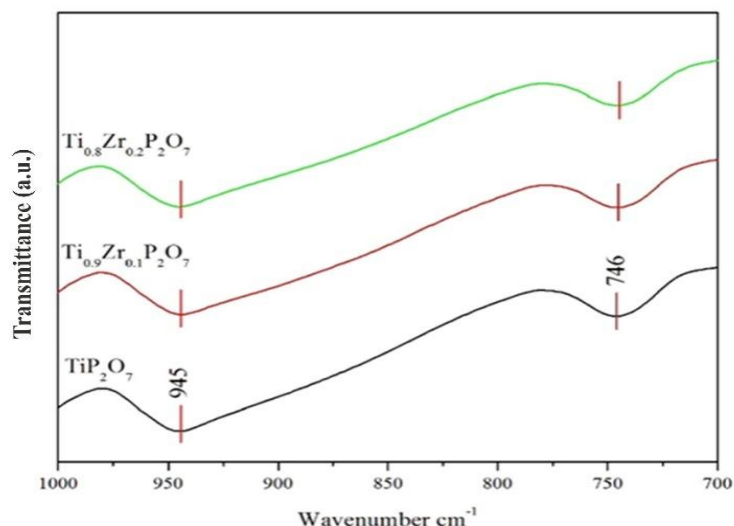


Figure 10: FT-IR spectra of TiP_2O_7 ($1000\text{-}700\text{ cm}^{-1}$)

The various vibration modes of the (PO_3) group and the POP bridge of various compounds, with frequencies and associated references are compiled in Table 3.

Table 3: Assignment of FT-IR bands for the studied compounds

Mixed phosphates	Vibration mode	Wave numbers (cm^{-1})	References
ZrP_2O_7	$\nu_{\text{as}}(\text{PO}_3)$	1271 and 1217	18,19
	$\nu_{\text{s}}(\text{PO}_3)$	1088 and 1047	17,18
$\text{Zr}_{0.9}\text{Ti}_{0.1}\text{P}_2\text{O}_7$	$\nu_{\text{as}}(\text{P-O-P})$	960	18
	$\nu_{\text{s}}(\text{P-O-P})$	748	18
$\text{Zr}_{0.8}\text{Ti}_{0.2}\text{P}_2\text{O}_7$	$\delta(\text{PO}_3)$	576, 541, 450 and 426	9,17
TiP_2O_7	$\nu_{\text{as}}(\text{PO}_3)$	1276	18,19
	$\nu_{\text{s}}(\text{PO}_3)$	1029	19
$\text{Ti}_{0.9}\text{Zr}_{0.1}\text{P}_2\text{O}_7$	$\nu_{\text{as}}(\text{P-O-P})$	945	19
	$\nu_{\text{s}}(\text{P-O-P})$	746	17,19
$\text{Ti}_{0.8}\text{Zr}_{0.2}\text{P}_2\text{O}_7$	$\delta(\text{PO}_3)$	615, 557 and 437	19

Synthesis of mixed phosphates of tetravalent elements is possible through various methods leading to different formulations and structural properties depending on the nature of metal precursor, phosphorus provider and the type of solvent when operating with precursors solutions. In this work, overall results described show the effectiveness of dry method (solid-state thermal synthesis [20]) for the preparation of well-defined formulations of Zr and Ti mixed phosphates starting from ZrO_2 and TiO_2 as metal precursors. A good control on the desired Zr/Ti ratios obtained for a substitution rate of Zr by Ti (or Ti by Zr) reaching 0.2. The limit of substitution rate performed (ca. 20%) is comparable to earlier studies using precursors solution for the substitution of Zr^{4+} in ZrP_2O_7 by Ti^{4+} , Sn^{4+} , Pb^{4+} or Ce^{4+} [20]. The change observed in unit cell parameters between mono and bimetallic pyrophosphates depended on the degree of substitution for $\text{Zr}_x\text{Ti}_{1-x}\text{P}_2\text{O}_7$ as a result of interchange between elements of different atomic radius. The pyrophosphate preparation from metal oxides and using solid-state synthesis selectively forms a unique $\text{Zr}_x\text{Ti}_{1-x}\text{P}_2\text{O}_7$ ($x < 0.2$ or $x > 0.8$) phase for temperatures not exceeding 900°C (instead of $T > 1200^\circ\text{C}$ for conventional solvent-assisted methods [21,22]). In the optimum range of successful formulation, no significant change was observed in crystal structure between ZrP_2O_7 and TiP_2O_7 single metal pyrophosphates and their bimetallic $\text{Zr}_x\text{Ti}_{1-x}\text{P}_2\text{O}_7$ counterparts. The free-solvent synthesis method opens new alternatives to conventional methods using metal salts solutions.

Conclusion

New pyrophosphate materials $Zr_xTi_{1-x}P_2O_7$ ($0 < x < 1$) were prepared from ZrO_2 and TiO_2 metal precursors and in the presence of $(NH_4)_2HPO_4$ as phosphate provider. The solid-state synthesis route was operated without the need to use solvent. In this process, a suitable heat treatment allowed the formation of well-defined mixed $Zr_xTi_{1-x}P_2O_7$ pyrophosphate phases for a Zr substitution rate by Ti (and vice versa) ($x < 0.2$ or $x > 0.8$). These new developed pyrophosphate phases were revealed by X-ray diffraction XRD, SEM scanning electron microscopy and infrared spectroscopy FT-IR demonstrating the presence of both characteristic bands associated with the vibration modes of (PO_3) groups and those of the pyrophosphate showing P-O-P bridge-like configuration. Deeper analysis of X-ray diffraction data shows that the substitution process takes place without change in the crystal structure for $Zr_xTi_{1-x}P_2O_7$ ($0 < x < 0.2$ or $0.8 < x < 1$) mixed pyrophosphates compared to ZrP_2O_7 or TiP_2O_7 single metal pyrophosphates. $Zr_xTi_{1-x}P_2O_7$ pyrophosphate matrix developed can be considered as potential model compounds to be applied in heavy metals trapping. We are also carrying out investigations to determine dielectric, electrochemical, magnetic and physicochemical properties of these new mixed pyrophosphates $Zr_xTi_{1-x}P_2O_7$ for their application in electromagnetism or electro-catalysis.

References:

1. Health risks of heavy metals from long-range transboundary air pollution, *Annual report of World Health Organization* (2007).
2. Biney C., Amuzu A.T., Calamari D., Kaba N., Mbome I.L., Naeve H., Ochumba O., Osibanjo O., Radegonde V., Saad M.A.H., *FAO fisheries report*, (1992).
3. Laganier D., *Caractérisation, stabilisation et valorisation des phosphogypses marocains*, Sherbrooke (Québec) Canada, (2002).
4. 1ères Assises nationales de R&D autour des phosphates, *Skhirat 13 septembre 2013*.
5. Aklil A., Mouflih M., Sebti S., *J Hazard Mater.*, 8(2004), 112(3), 183-90.
6. Hutchings G.J., *J Mater. Chem.*, 19(2009)122-1235.
7. Sqalli O., Malaman B., Ijjaali M., *Materials Letters*, 58 (2004) 2984–2987.
8. Sqalli O., Oulmekki A., Ijjaali M., Malaman B., Laouini M., *Materials Letters* 59 (2005) 1329–1333.
9. Oulmekki A., « *Contribution à l'étude du système M-P-O : synthèse, structure et propriétés physico-chimiques des nouveaux phosphates $FePb_2(P_2O_7)(PO_4)$, $Fe_2Pb_3(PO_4)_4$, $MgFe_2(P_2O_7)_2$, $CoFe_2(P_2O_7)_2$, $Co_5Fe_2(P_2O_7)_4$* », *Faculté des sciences Oujda. Université Mohamed I^{er}*, Thèse (2002).
10. Kinomura N., Hirose M., Kumada N., Muto F., *Mat. Res. Bull.*, 20 (1985) 379-382.
11. Parhi P., Kramer J. W., Manivannan V., *Materials Science and Engineering B* 153 (2008) 53–56.
12. Shi Z., Wang Q., Ye W., Li Y., Yang Y., *Microporous and Mesoporous Materials* 88 (2006) 232–237.
13. Levi G. R., Peyronel G., *Zeitschrift fuer Kristallographie, Kristallgeometrie, Kristallphysik, Kristallchemie* 144(1977), 1935, 92, 190-209.
14. Norberg S. T., Svennson G., Albertsson J., *Acta Crystallographica Section C*, 57 (2001) 225-227.
15. Zhou L., *E-Journal of Chemistry*, 9(3) (2012) 1320-1326.
16. Hao Y., Wu C., Cui Y., Xu K., Yuan Z., Zhuang Q., *Ionics*, 20 (2014) 1079.
17. Lai Y., Liang X., Yang S., Liu P., Zeng Y., Hu C., *J. of Alloys and Compounds*, 617(2014) 597-601.
18. Stefanovsky S.V., Stefanovsky O.I., Kadyko M.I., *J. of Non-Crystalline Solids*, 443 (2016) 192-198.
19. Santha N., Nayar V. U., Keresztijry G., *Spectrochimica Acta*. 49A (1993) 41-52.
20. Ijjaali M., Venturini G., Gerardin R., Malaman B., Gleitzer C., *Eur. J. Solid State Inorg. Chem.*, 28(1991) 983.
21. Ota T., Yamai I., *J. Mater. Sci.*, 22 (1987) 3762–3764.
22. Wang S., Jiang X., Du G., Guo Z., Jang J., Kim S.J., *Materials Letters*, 65(2011) 3265–3268.

(2017) ; <http://www.jmaterenvironsci.com>